BIOCHEMISTRY
including biophysical chemistry & molecular biology

Article

pubs.acs.org/biochemistry

Role of the Central Arginine R133 toward the Ion Selectivity of the Phosphate Specific Channel OprP: Effects of Charge and Solvation

Niraj Modi,[‡] Iván Bárcena-Uribarri,[‡] Manjeet Bains,[§] Roland Benz,[‡] Robert E. W. Hancock,[§] and Ulrich Kleinekathöfer*[,‡]

[‡]School of Engineering and Science, Jacobs University Bremen, Campus Ring 1, 28759 Bremen, Germany

[§]Centre for Microbial Diseases and Immunity Research, Department of Microbiology and Immunology, University of British Columbia, Vancouver, Canada

Supporting Information

ABSTRACT: The outer membrane porin OprP of *Pseudomonas aeruginosa* forms a highly specific phosphate selective channel. This channel is responsible for the high-affinity uptake of phosphate ions into the periplasmic space of the bacteria. A detailed investigation of the structure−function relationship of OprP is inevitable to decipher the anion and phosphate selectivity of this porin in particular and to broaden the present understanding of the ion selectivity of different channels. To this end we investigated the role of the central arginine of OprP, R133, in terms of its effects in selectivity and ion transport properties of the pore. Electrophysiological bilayer measurements and free-energy molecular dynamics simulations were carried out to probe the transport of different ions through various R133 mutants. For these mutants, the change in phosphate binding specificity, ion conduction, and anion selectivity was determined and compared to previous molecular dynamic calculations and electrophysiological measurements with wild-type OprP. Molecular analysis revealed a rather particular role of arginine 133 and its charge, while at the same time this residue together with the network of other residues, namely, D94 and Y114, has the ability to dehydrate the permeating ion. These very specific features govern the ion selectivity of OprP.

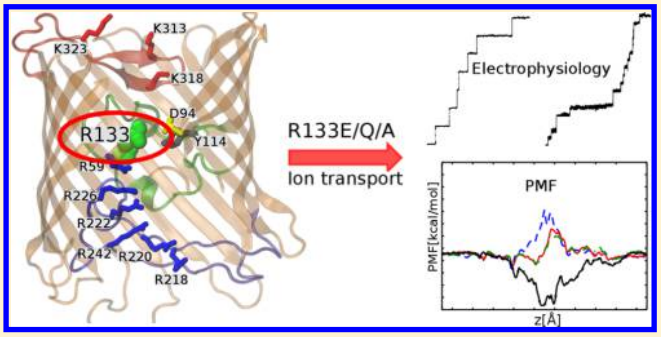

The outer membranes of Gram-negative bacteria act as molecular filters. The filter function is mainly due to the presence of a certain class of membrane proteins called porins.[1] Porins have a β-barrel architecture and form water-filled, membrane-spanning channels that permit the passage of charged and neutral solutes including ions across the bacterial outer membrane into the periplasmic space. Most porins form relatively nonspecific general diffusion pores (e.g., OmpF and OmpC of *Escherichia coli*), whereas some act as substrate-specific channels such as those selectively transporting carbohydrates (LamB and ScrY of *E. coli*, OprB of *Pseudomonas putida*), nucleosides (Tsx of *E. coli*), or phosphate ions (OprP of *Pseudomonas aeruginosa*).[1] A molecular analysis of the substrate specificity of these porins is inevitable in order to understand the corresponding structure−function relationship as this has major implications that go far beyond biological systems, for example, in the design of substrate-specific synthetic nanopores with diverse functions.[2,3] Electrophysiological experiments complemented by all-atom molecular dynamics simulations provide an excellent platform to investigate the functions and selectivity of these porins and to understand, for example, ion[4−9] or antibiotics transport.[10−13]

Under phosphate limitation or starvation conditions, *P. aeruginosa* induces the protein OprP in its outer membrane for high-affinity uptake of phosphate ions.[14] The selectivity of OprP for phosphate represents an interesting example of substrate specificity for which various details are still unknown. The OprP channel is an exception among the substrate-specific porins because of its anion selectivity and in particular because of its high phosphate selectivity. The OprP crystal structure reveals a trimeric form of the porin in which each monomer consists of 16 β-strands and extracellular, as well as periplasmic loops.[15] In particular, the loops L3, L5, and T7 fold into the lumen of the pore and are responsible for the constriction regions inside the pore (Figure 1a). Important structural features that determine the anion selectivity of the channel are the so-called arginine ladder including residues R218, R220, R242, R222, R226, R59, R60, and R34 that extends from the extracellular side down the channel to the middle of the pore and a lysine cluster including residues K13, K15, K25, K30, K74, K109, K313, K323, and K378 on the periplasmic side of the channel (see Figure 1). Two central phosphate binding sites are formed by residues D94, Y62, S124, S1235, K121, K126, R34, and R133.[15]

Received: April 26, 2013
Revised: July 19, 2013
Published: July 22, 2013

   dx.doi.org/10.1021/bi400522b | *Biochemistry* 2013, 52, 5522−5532

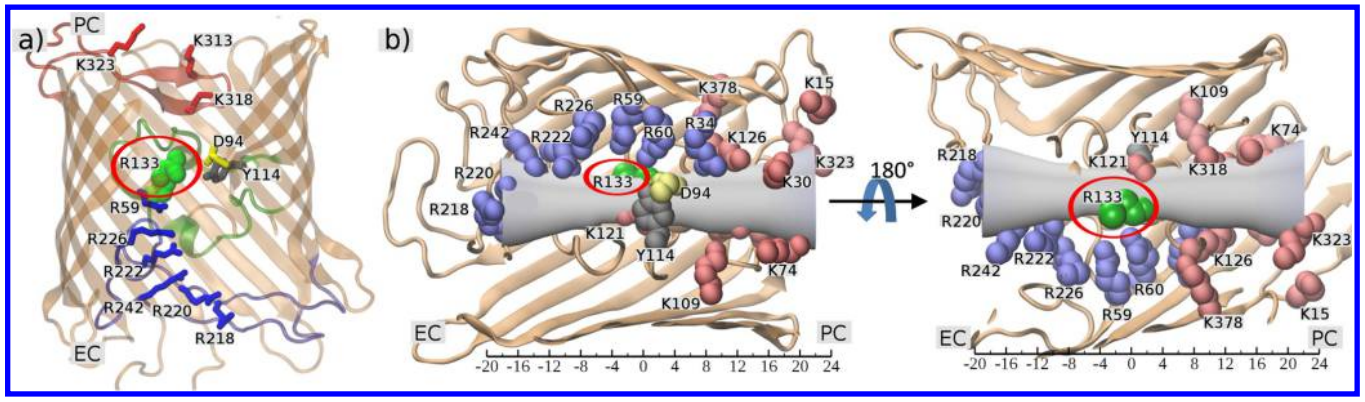

Figure 1. Structural features of OprP. (a) An OprP monomer is shown with loops L3 (green), L5 (blue), and T7 (red), which lead to a narrow pore. Important residues along the pathway of the pore are shown as sticks (Arg - blue, Lys - red, Asp - yellow, Tyr - gray) and Arg133 as green colored spheres. EC and PC denote the extracellular and periplasmic sides of the pore, respectively. (b) The monomer pore is shown together with a gray hourglass shape to demonstrate the approximate radius of the pore in the different regions and to indicate a possible ion permeation pathway. Important residues, including Arg133, are labeled and mapped to their position along the *z* axis.

Table 1. Mutants Designed to Study the Role of the Amino Acid R133 in Ion Selectivity and Phosphate Substrate Specificity[a]

OprP	codon	5′-3′ Primer	protein side chain
R133 (WT)	CGC	not mutated	$-CH_2-CH_2-CH_2-NH-C(NH_2)-NH$
R133E	GAG	CCGCGCTGGAG**GAG**AACCTCACCTACG	$-CH_2-CH_2-COOH$
R133Q	CAG	CACCGCGCTGGAG**CAG**AACCTCACCTAC	$-CH_2-CH_2-CO-NH_2$
R133A	GCC	CCGCGCTGGAG**GCC**AACCTCACCTACG	$-CH_3$

[a]The codons of the wild type and mutants are indicated as well as the primers used to mutate them. The side chains of the different amino acids are also shown.

Our previous electrophysiological experiments suggested that phosphate permeation is ∼20 higher than the chloride transport.[16−18] This was largely attributed to an 100−500 fold higher binding affinity of OprP for phosphate compared to chloride. Recently, we also probed the ion selectivity of wild-type OprP utilizing all-atom molecular dynamics free-energy calculations.[19] In that study, the transport properties of various ions was compared by determining the potential of mean force (PMF) profiles. Molecular details for the selectivity of OprP were revealed and also discussed in the context of well-studied ion channels such as potassium or chloride selective channels. The porin OprP and especially its selectivity was also investigated by Sansom and co-workers using molecular dynamics simulations[20] and employed as a template for possible artificial nanopores.[21]

To enable further understanding of the structure−function relationships of this specific porin, the contributions of individual residues, that are likely to be relevant to the selectivity of OprP, need to be investigated. To this end, we investigated the role of one of the most important residues of the central binding sites, arginine 133 (R133), toward the selectivity of OprP. R133 is strategically located in the central region of the pore (see Figure 1) and is reported to form interactions with the phosphate ion in both central binding sites.[15] Its positive charge, large side chain, and H-bond donor capacity make it probably one of the most influential residues for controlling the selectivity and governing the corresponding molecular interactions. In addition, its functional importance is also evident in the evolutionary process as R133 is conserved among the orthologs of OprP in different *Pseudomonas* species (see Supporting Information). Three mutants of OprP were generated as listed in Table 1: R133E (charge inversion - positive to negative charge), R133Q (positive to neutral charge, large side-chain compared to alanine), and R133A (positive to neutral charge, small side chain) where the letters R, E, Q, and A represent the amino acids arginine, glutamate, glutamine, and alanine, respectively. Electrophysiological experiments with planar lipid bilayer were performed to understand the transport of different ions through OprP and to obtain binding constants for phosphate-mediated inhibition of chloride transport. These experiments were complemented by free-energy molecular dynamics simulations to probe the molecular details. The findings were compared with results for wild-type (WT) OprP to understand the contribution of R133 toward the selectivity of OprP.

MATERIALS AND METHODS

Experimental Details. *Bacterial Strains and Growth Conditions.* *E. coli* strain DH5α (Invitrogen, CA, United States) was used as a host for clones containing the OprP expression plasmid pAS27[22] and the various plasmids containing OprP single mutations. *E. coli* CE1248,[23] which lacks the major porins OmpC, OmpF, and PhoE, was used in all expression studies to facilitate the purification of the OprP mutants. *E. coli* CD1248 cells harboring the various plasmids were inoculated from Luria−Bertania agar plates (Fisher Scientific, Canada) containing 100 μg/mL ampicillin (Sigma, Canada) directly into 1.0 L of Luria−Bertani broth supplemented with 100 μg/mL ampicillin and 0.4% glucose to impede the expression of LamB. The cells expressing the different OprP mutants were induced once they reached an OD600 of 0.5−0.8 with 0.8 mM of IPTG and further cultivated overnight. Afterward, the cells were harvested by centrifugation at 8000*g* for 10 min.

Site-Directed Mutagenesis and Sequencing of OprP Mutants. The pAS27 plasmid was individually mutated using the Quick-Change mutagenesis kit (Stratagene, USA) following

dx.doi.org/10.1021/bi400522b | *Biochemistry* 2013, 52, 5522−5532

the manufacturer instructions. The primers used to perform the single mutations are described in Table 1. For each amino acid substitution, two complementary primers containing the desired mutation were designed according to guidelines in the QuikChange XL Site-directed Mutagenesis manual and synthesized by AlphaDNA (Montreal, Canada). Mutagenic codons containing mismatches that corresponded to the substitution mutation in the encoded amino acid sequence of OprP are also listed in Table 1. Each of the mutagenized OprP constructs was sequenced by the Nucleic Acid Protein Service Unit (University of British Columbia, Vancouver, Canada) to ensure they had the correct mutant sequence and no additional mutations.

Protein Extraction and Purification. The *E. coli* CE1248 pellets obtained after cultivation were resuspended in 10 mM Tris-HCl pH 8.0 containing 20% sucrose and 50 μg/mL DNase 1. The resuspended cells were incubated at 23 °C for 10 min and then placed on ice and lyzed two times by passage through a French pressure cell at 15 000 psi; unbroken cells were removed by centrifugation at 5000*g* for 10 min at 4 °C. The supernatants were layered onto a 2-step sucrose gradient (50% and 70%) and centrifuged in a SW28 swinging bucket rotor at 23 000 rpm for 18 h at 4 °C. Once the fraction containing the outer membranes was collected, the concentration of sucrose was diluted to below 20% with distilled water, and the membranes were pelleted in an ultracentrifuge at 41 000 rpm at 4 °C for 1 h. The outer membranes were then washed once with water. The proteins present in the outer membranes were solubilized first with a buffer containing 10 mM Tris HCl pH 8.0 and 3% tetraoxyethylene *n*-octyl ether (C8E4) (Bachem Inc., USA), followed by this buffer with the addition of 10 mM EDTA, pH 8.0 and then with added 1.0 M NaCl. The solubilized fractions were analyzed by SDS-PAGE, and OprP was predominantly found in the fraction solubilized with 10 mM Tris-HCl pH 8.0, 3% C8E4, and 10 mM EDTA. The selected fraction was then diluted to obtain a final C8E4 concentration of 0.6%. Subsequently, the OprP native and mutant proteins were purified using a NaCl gradient applied to a MonoQ column on a FPLC system (Pharmacia, United States). The OprP protein eluted at a salt concentration of 250−300 mM NaCl. The presence of the protein was checked using SDS-PAGE and Western immunoblotting.

Sodium Dodecyl Sulfate-Polyacrylamide Gel Electrophoresis (SDS-PAGE) and Western Immunoblotting (WB). To check the expression of the OprP mutants and its purification, whole cell lysates of *E. coli* CE1248 or the FPLC fractions were loaded onto a 12% SDS polyacrylamide gel and electrophoresed. The gels were stained with Coomassie blue or transferred to polyvinylidene fluoride (PVDF) membranes and incubated with monomer-specific anti-OprP rabbit serum as previously described.[22] *E. coli* CE1248 harboring pAS27 was used as a positive control and *E. coli* CE1248 harboring the vector plasmid pTZ19U (Pharmacia, USA) was used as a negative control.

Black Lipid Bilayer: Single Channel Conductance, Zero Current Measurements, and Phosphate Titration. The black lipid bilayer assay has been previously described.[24] An artificial membrane was spread over a 0.5 mm^2 hole dividing two compartments of a Teflon cuvette. The artificial membranes were formed using a solution of 1% diphytanoylphosphatidylcholine (DiPhPC) in *n*-decane (Avanti Polar Lipids, Alabaster, AL). Both compartments are filled with a salt solution (0.1 M KCl). Two Ag/AgCl electrodes with salt bridges switched in series were immersed in each compartment of the membrane cell. One of the electrodes was connected to a homemade voltage source and the other to a homemade amplifier/filter based on a Burr-Brown operational amplifier. The output signal of the amplifier was monitored with a digital oscilloscope and a strip chart recorder (Rikadenki Electronics, Germany). For single channel conductance and titration experiments, a +50 mV voltage was applied to the electrode connected to the voltage source.

Measurements to study inhibition of chloride conductance mediated by phosphate binding to the binding sites were performed for OprP and the R133 mutants as previously described.[25,26] The aqueous phase contained 0.1 M KCl, 10 mM MES at pH 6 in these experiments. The protein was added to the membrane cell under stirring conditions. The membrane conductance increased for about 30 min due to reconstitution of OprP and its mutants. Once the conductance was stable and did not increase further, at that time small amounts of concentrated phosphate solutions (pH 6) were added to both sides to study inhibition of chloride conductance by binding of phosphate to the binding site. This could be detected by the reduction of the membrane conductance. After progressive increments of the phosphate concentration under stirring, the half saturation constant for chloride conductance through OprP and its mutants as mediated by phosphate binding was calculated using the Michaelis−Menten equation.[25,27]

Zero current measurements to study the ion selectivity were performed as described elsewhere.[24,28] An electrochemical gradient was progressively established by adding a 0.5 M KCl, LiCl, or KAc solution to the cis-side and 0.1 M of the same salt to the trans-side of the membrane cell. The aqueous salt solutions were buffered with 10 mM HEPES, pH 6, if not indicated otherwise, T = 20°. The generated potentials were measured with a high-impedance electrometer (Keithley 617) connected to the trans-side electrode under zero current conditions.

Computational Details. *Molecular Dynamics System Setup.* A trimer of OprP (PDB code 2O4V)[15] was embedded into a palmitoyloleoyl-glycero-phosphathidyl ethanolamine (POPE) lipid bilayer that was constructed from pre-equilibrated patches using VMD.[29] Subsequently, the system was solvated using TIP3P water molecules. The R133 residues in each of the monomers were mutated to glutamate (E), glutamine (Q), or alanine (A) to generate the three mutant systems R133E, R133Q, and R133A, respectively. Each of the three systems was subjected to 5000 steps of energy minimization to remove unfavorable sterical contacts followed by a ∼5 ns equilibration run. One of the three studied ions (phosphate, chloride, and potassium) was subsequently placed at the mouth of the one of the monomers on the extracellular side for each of the mutants (nine different systems systems considering the different combinations between three ions and three mutants). As already done in our WT OprP study,[19] the monovalent form of the phosphate ion, $H_2PO_4^-$, was chosen since phosphate is predominantly monobasic at pH 6 of experimental measurements. All nine systems were neutralized by addition of potassium ions and each system contained ∼120 000 atoms.

Molecular Dynamics Simulation Parameters. The simulations were performed in the NPT ensemble with the program NAMD 2.8[30] and the CHARMM27 force field[31] along with additional force field parameters for $H_2PO_4^-$.[32] The temperature of 310 K and the pressure of 1 atm were maintained in all

dx.doi.org/10.1021/bi400522b | *Biochemistry* 2013, 52, 5522−5532

the simulations using Langevin dynamics along with a Langevin piston algorithm. Periodic boundary conditions were used in the simulations. Short-range nonbonded interactions were calculated using a cutoff of 12 Å and a switching distance of 10 Å. The long-range electrostatic interactions were accounted for using the particle mesh Ewald method.[33] Bonded interaction were evaluated every 1 fs. Short-range nonbonded and long-range electrostatic interactions were evaluated at every 2 and 4 fs respectively using the r-RESPA multiple time step method.[34] Bond constraints were applied to all water hydrogen atoms with the SHAKE algorithm.[35]

Free Energy Calculations. The adaptive biasing force (ABF) approach[36−38] as implemented in the *collective variable* module of the NAMD 2.8 program[30] was applied to determine the effective free energy profiles for the transport of different ions through OprP mutants. The principal axis of the channel was aligned parallel to the z axis, and the reaction coordinate was assigned to be the z position of the ion. Moreover; the change in free energy was determined with respect to the bulk value. The full reaction coordinate with a length of ∼84 Å along the z axis was subdivided into 21 windows with a length of 4 Å each to enhance the sampling efficiency. This range of reaction coordinate along the z axis also consisted of extended bulk regions on both sides of the channel. The initial starting conformations of the system for each window were retrieved by constant velocity steered molecular dynamics (SMD) simulations wherein each studied ion was dragged through the channel along the z axis. In the ABF method, the average force acting on the respective ion was accumulated in 0.1 Å sized bins within each window. In addition, the application of the adaptive bias was initiated only after 800 samples were accumulated in the individual bins to address the issue of the fluctuations of the instantaneous forces and to calculate a reasonable starting estimation of the biasing forces. Later on, the resulting data were integrated to generate the potential of mean force (PMF) profiles. Production runs in each window were carried out for at least 6 ns while considerably extended runs were performed for about 15−20 ns in the central binding site windows (−10 to 10 Å). This led to production runs of ∼160 ns for each ion and a total simulation time of ∼1.4 μs for all nine systems in total (three ions and three mutants).

RESULTS AND DISCUSSION

As shown in Table 2, electrophysiological bilayer experiments showed that the single channel conductance (G) of the OprP channel suffered an extreme reduction for all of the three mutants. The channel conductance went down from 160 pS in 0.1 M KCl measured for the wildtype (WT) protein to a conductance of between 5 and 12 pS for the three R133 mutants. Furthermore, a drastic increase of the apparent dissociation constant (half saturation constant, 1/K) was observed when the OprP mutants were used to study the inhibition of chloride conductance by adding phosphate to the membrane cell (Table 2). Charge inversion mutation, R133E, and the mutation of arginine to neutral alanine with a small side chain, R133A, led to to the weakest inhibition of chloride conductance by phosphate with ∼40 increase of the half saturation constant as compared to WT (Table 2). The other mutation, R133Q, in which positively charged arginine was replaced by the neutral glutamine with a large side chain, also resulted in a weaker binding of phosphate with an increase of the half saturation constant by a factor of about 30 (Table 2). These findings indicate the critical importance of the positive charge at this particular position of OprP in assigning the high phosphate specificity to the pore. If the length of the side chain had any effect on phosphate binding is difficult to say because electrostatic effects seem to play an extremely high role in the phosphate binding process. It is also difficult to say if a significant difference exists in half saturation constants between all three R133 mutants.

Table 2. Single Channel Conductance and Half Saturation Constants of Chloride Conductance Inhibition by Phosphate Binding for WT OprP and Mutants[a]

OprP	G (pS) (KCl)	half saturation constants of chloride conductance inhibition by phosphate (1/K) (10^{-3} M)	stability constants of chloride conductance inhibition by phosphate (K) (1/M)
R133 (WT)	160	1.2	820 ± 160
R133E	8	45	22 ± 1.8
R133Q	5	33	30 ± 2.2
R133A	12	50	20 ± 1.9

[a]The single channel conductance was obtained in 0.1 M KCl, 10 mM MES, pH 6, T = 20 °C and applying 50 mV voltage. The stability constant for chloride conductance inhibition by phosphate was obtained from titration experiments with the OprP WT and mutant channels mediated conductance, using the Michaelis−Menten equation described elsewhere.[25] The phosphate solution had a pH of 6. Mean value of at least three individual titration experiments are shown.

Additionally zero current measurements were carried out to study possible changes in the ion selectivity of the R133 mutants compared to the WT. After a 5-fold concentration gradient was established across the membrane, the electrical potential difference was measured using an electrometer. In previous studies,[18] the WT OprP protein displayed an anion to cation permeability ratio, P_a/P_c, of greater than 70 in KCl (Table 3). Hydrated K^+ and Cl^- have approximately the same hydrodynamic radius and therefore a similar size. This permeability ratio indicates a clear preference of the OprP channel for anions. In a similar manner, the ion selectivity in KCl was also analyzed for the R133 mutants in this study. R133E/Q/A mutants retained the overall anion selectivity of the channel. However, the mutants showed a decrease in anion selectivity with the permeability ratio, P_a/P_c, dropping from >70 for the WT to about 20−30 for the different mutants as listed in Table 3. The decrease of selectivity between OprP wildtype

Table 3. Zero-Current Measurements To Study the Ion Selectivity of OprP and the R133 Mutants[a]

	permeability ratios P_a/P_c (V_m [mV])			
electrolyte	R133	R133E	R133Q	R133A
KCl	>70[18]	28 (−37.3 ± 0.9)	17 (−35.1 ± 3.6)	29 (−37.4 ± 2.4)
LiCl	>100	22 (−36.3 ± 0.6)	25 (−36.9 ± 1.9)	15 (−34.3 ± 1.0)
KAc (pH 7)	>100	6 (−27.0 ± 0.3)	62 (−39.4 ± 0.4)	32 (−37.7 ± 1.3)

[a]The experiments were carried out for five-fold gradients (0.1 M versus 0.5 M) of three different salts. The ratio of anions to cations permeability, (P_a/P_c) was calculated using the Goldmann−Hodgin−Katz equation[24] from at least three individual experiments. The zero-current membrane potential, V_m, is defined as the difference between the potential at the dilute side and the concentrated side of salt solutions.

dx.doi.org/10.1021/bi400522b | *Biochemistry* 2013, 52, 5522−5532

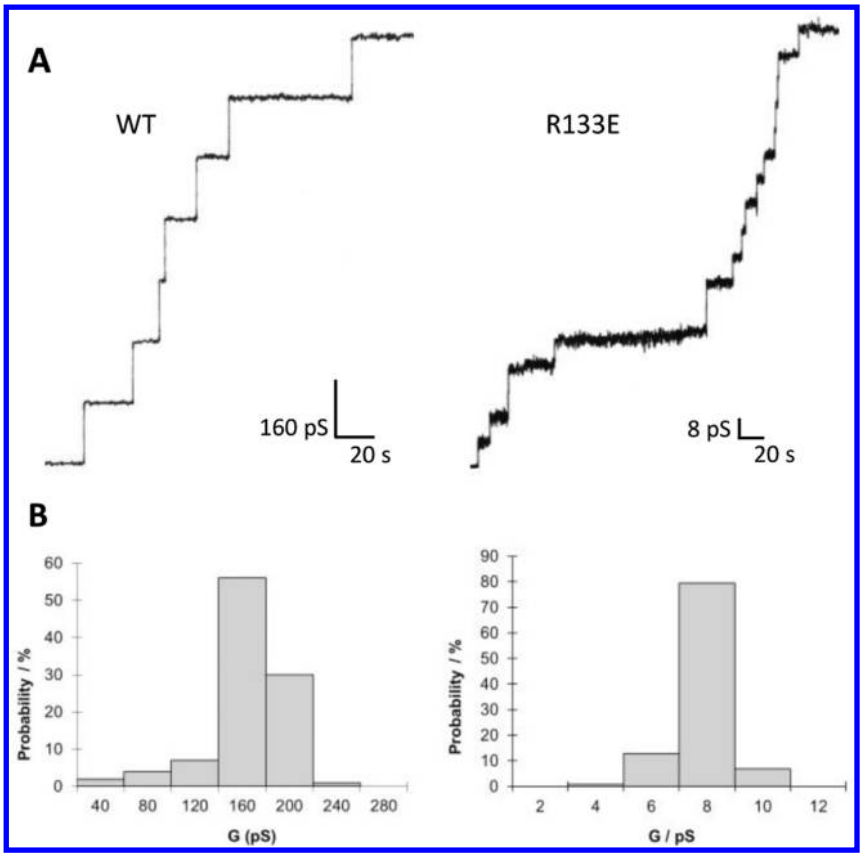

Figure 2. Single channel activity of OprP wildtype (WT) and the R133E mutant. (A) Step-wise increase in conductance produced by individual insertions in a DiPhPC membrane. Time and conductance for each measurement are shown by the scale. Different scales were used to optimize the resolution of the single channel conductance for each sample. (B) Histograms summarizing the conductance (G) in picosiemens (pS) of the single channel events observed for WT OprP (left) and R133E mutant (right). The measurements were performed in 0.1 M KCl, 10 mM MES, pH 6, 20 °C with an applied voltage of 50 mV.

and the three R133 mutants is significant. However, the zero-current membrane potentials (V_m) observed with all three mutants are in a range where small errors in the potential measurements result in large changes in the permeability ratio. Therefore, the differences in the permeability ratios between the three R133 mutants have to be interpreted with care also taking the standard deviations in the zero-current membrane potentials into account. To support the results obtained for KCl, the measurements were repeated using lithium chloride (LiCl) and potassium acetate (KAc). Also for these salts, the R133 mutants showed a decrease in the anion selectivity of the channel compared to WT.

To further probe the molecular factors behind the influence of R133 on the phosphate binding, all-atom free-energy molecular dynamics simulations were performed. One-dimensional potential of mean force (PMF) profiles were calculated (see Materials and methods for details) to quantify the changes in the free energy associated with the transport of the different ions through the OprP mutants R133E/Q/A. In a previous study, we had already derived similar profiles for the transport of ions through WT OprP.[19] Here we compare our new results obtained with mutants to the WT data to enable discussion of the relative contribution of R133 toward the ion selectivity of OprP. The PMF profile for the transport of $H_2PO_4^-$ through WT OprP had revealed two energetically favorable central binding site regions with an energy well depth of ~8 kcal/mol (see Figure 3a).[19] Contrary to the WT results, the $H_2PO_4^-$ transport through the R133E mutant indicated a complete inversion of the PMF profile in which the energetically favorable central binding site region was replaced by a central barrier with a height of ~7 kcal/mol as shown in Figure 3a. R133E is a charge inversion mutation in which the positive charge of arginine was replaced by the negative charge of glutamate. This numerical finding already demonstrates the importance of residue R133 in making phosphate transport through the OprP channel energetically favorable.

Subsequently R133 was mutated to the neutral glutamine (Q) with a relatively large side chain and the similarly neutral alanine (A) but with a very small side chain to further understand the effect of charge and size of the residue. The R133Q and R133A mutants also showed a barrier to $H_2PO_4^-$ transport, albeit the barrier heights were smaller, i.e., 4 and 3 kcal/mol for R133Q and R133A, respectively, cf. that of R133E showing a 7 kcal/mol barrier (see Figure 3a). Changes in the charge of a residue at position 133 from positive (R) to neutral (Q or A) to negative (E) and the associated large changes in the PMF profiles for the $H_2PO_4^-$ transport are a strong indication of the importance of specific charges toward the ion selectivity at this particular position of OprP. Moreover, the barrier height for R133Q was ~1 kcal/mol higher than that for R133A, which indicates the influence, on ion-selectivity and transport, of the size of the side chain and consequently steric factors, albeit that the effect was small compared to the charge effects. In addition, based on the PMF profiles, we calculated the dissociation constants ($1/K$) for the $H_2PO_4^-$ transport through OprP mutants to compare with experiments. To this

dx.doi.org/10.1021/bi400522b | *Biochemistry* 2013, 52, 5522−5532

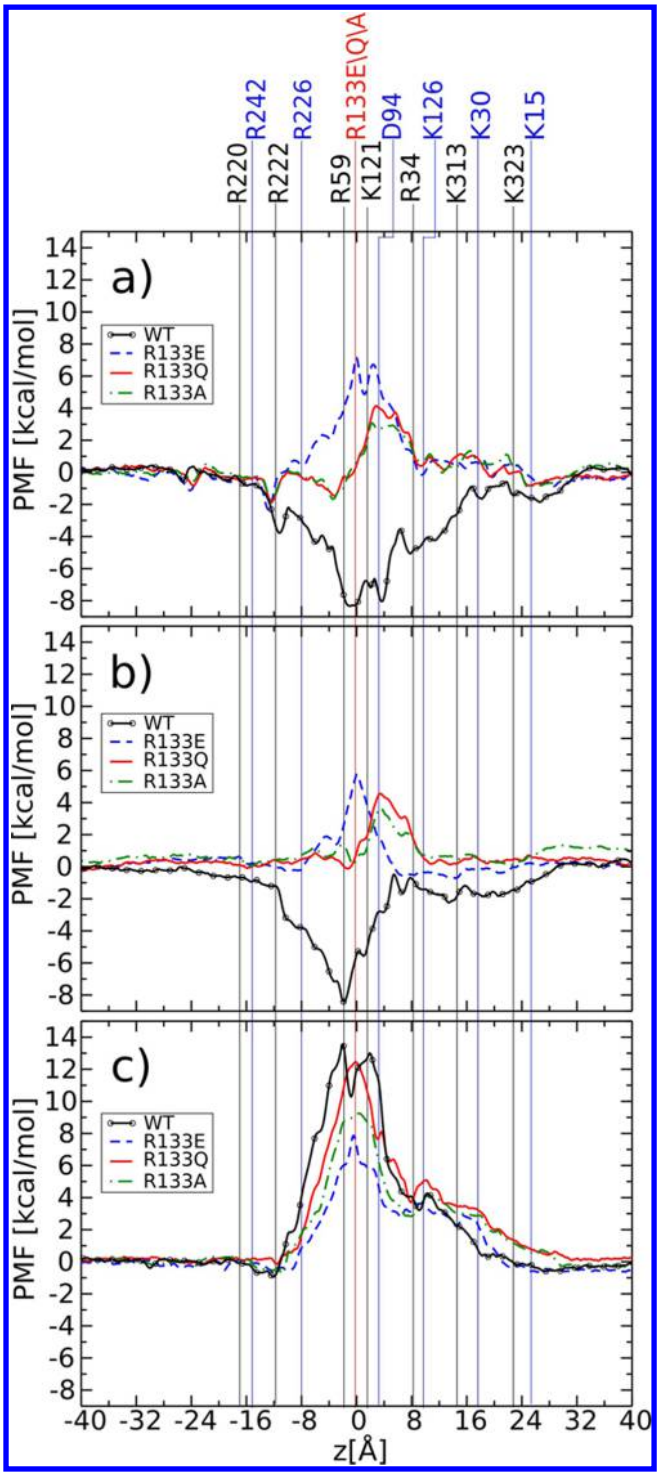

Figure 3. PMF profiles for the permeation of (a) $H_2PO_4^-$, (b) Cl^-, and (c) K^+ ions through the OprP mutants R133E, R133Q, and R133A. The PMFs for the WT channel are shown for comparison.[19] Important residues of OprP along the ion permeation pathway are mapped onto the PMF profiles with respect to their positions along the z axis.

end, the same method discussed in ref 19 was used to calculate the dissociation constants. The calculated dissociation constants were found to be 8.6 mM, 3.82 mM, 5.4 mM, and 0.23 μM for R133E, R133Q, R133A, and WT OprP, respectively. While these values were not in quantitative agreement with the experimentally determined half saturation constants, qualitatively they showed a similar trend. For example, in simulations we observed a drastic reduction in phosphate binding affinity from WT OprP to all R133 mutants as was the case with experiments (Table 2). In addition, the difference between the binding affinity of phosphate to the three R133 mutants is not significant in simulations which is in agreement with the experiments (Table 2).

Cl^- transport through the R133E mutant (Figure 3b) also showed an inversion of the PMF with a barrier height of ~6 kcal/mol. The WT OprP channel had a single central binding site with a well depth of ~8 kcal/mol.[19] In contrast, the R133Q and R133A mutations resulted in barrier heights of approximately 4 and 3 kcal/mol for Cl^-, respectively. The qualitative rank order of the barrier heights among the studied mutants for the Cl^- transport was consistent with that assessed for the $H_2PO_4^-$ ion. The R133E mutant has the highest barrier height and the R133A variant the lowest. These Cl^- transport findings can be interpreted in a manner similar to that for the $H_2PO_4^-$ transport, indicating the effects of charge and steric factors on the PMF profiles. Here we would like to point out that PMF calculations for membrane proteins are also reported to be affected by simulation details such as the finite system size and the use of nonpolarizable force fields especially for the lipid hydrocarbons of the membrane.[39] Sometimes these shortcomings might lead to overestimation of barrier heights. Since we are focusing on relative comparisons of PMF profiles, these problems will be much less severe in the present case. The PMF profiles for the $H_2PO_4^-$ and the Cl^- transport through R133 mutants consistently proved that any change in this particular residue led to a channel that was devoid of anion-binding capacity. This finding is also reinforced by the drastic reduction in experimental phosphate stability constants as listed in Table 2 for the R133 mutants.

Such drastic changes in PMF profiles for anions transport through the R133 mutants, particularly R133E, makes the transport of the cation, K^+, very intriguing. In our previous study of the WT pore,[19] K^+ had to overcome a huge energetic barrier of ~13 kcal/mol as seen in Figure 3c. It is interesting to examine if the R133E mutant can experience a similar PMF inversion for a cation as is observed for anions. As shown in Figure 3c, the PMF profile for K^+ transport through the R133E mutant revealed a reduction in the barrier height from 13 to 7 kcal/mol but not a complete PMF inversion. On the basis of these findings, it can be stated that the R133E mutation might be required to make the OprP channel cation selective but is not by itself sufficient. In the case of R133Q, the barrier height for K^+ transport was similar to that of the WT and has a value of 9 kcal/mol for the R133A mutant.

The PMF profiles for K^+ and Cl^- transport through R133 mutants also explained a drastic reduction in the KCl conductance from 160 pS for WT to 5−12 pS for mutants in electrophysiological experiments (see Table 2). Both K^+ and Cl^- ions have to pass energetic barriers in order to travel through the mutant pores which make their transport less favorable leading to a reduced conductance. While in the case of the WT channel, Cl^- had an energetically favorable binding site region within the pore, as depicted in Figure 3b, and a major part of the conductance is contributed by chloride ions. Moreover, the PMF profiles obtained are consistent with the ion selectivity measurements reported in Table 3 . The electrophysiological measurements indicated that the R133 mutants maintain a preference for anions, but this property is less pronounced than observed in the WT. The preference for

dx.doi.org/10.1021/bi400522b | *Biochemistry* 2013, 52, 5522−5532

anions of the respective mutant channels was supported by the PMF profiles whereby for all the R133 mutants, K^+ ions had a higher energetic barrier to pass than did the Cl^- ions (see Figure 3b,c). The reduced preference for anions by R133 mutants compared to WT OprP could be explained by the fact that in the WT channel, a large difference exists between PMFs of Cl^- and K^+, while in the case of mutants, these differences are less pronounced (Figure 3b,c).

In addition to the PMF profiles, the contribution of individual energy components, namely, the electrostatic and the van der Waals interactions, to the differential selectivity and binding of ions between various R133 mutants was determined. For this purpose, the pore was divided into 1 Å bins, and average energies between the permeating ion and the channel were calculated, with a cutoff distance of 12 Å using the NAMDenergy plugin. A similar analysis in our previous study with respect to the WT pore showed that the electrostatic components of the energy are the major factor in determining the anion selectivity of the channel, with minor contributions from the van der Waals interactions.[19] For the mutants also, the electrostatic interactions turned out to be the most dominating factor that impacted on the differential binding and selectivity of ions for the different mutants. The van der Waals interaction energies were very small (data not shown). In the case of $H_2PO_4^-$ transport through the R133E channel, the ion experienced unfavorable electrostatic interactions in the central region of the pore, in contrast to the very favorable energies obtained for the WT case as shown in Figure 4a. For R133Q/A, the electrostatic energy components were similar to the bulk region, but the $H_2PO_4^-$ ion certainly lost its energetic advantages demonstrated for the WT case (see Figure 4a). As shown in Figure 4b for Cl^- ions, similar trends could be observed in terms of electrostatic interactions between the ion and the channels of R133 mutants. In addition to electrostatic factors, entropic penalties associated with the confinement of ions and particularly for larger ions such as $H_2PO_4^-$ molecular ions,[40] as well as penalties due to dehydrating the ion may also contribute toward the overall barriers observed in the PMF profiles. The results for K^+ ions are displayed in Figure 4c. These ions experienced less unfavorable electrostatic interactions in the mutants compared to the WT channel, but a barrier nevertheless was evident as also reflected in the PMF profile.

One of the very interesting aspects of ion-selective channels from the perspective of an atomic analysis is the coordination number. It yields clues about the interactions and interplay between the permeating ions, surrounding water molecules, and the channel. Such analysis are widely exploited to derive a couple of hypotheses addressing the issue of ion-selectivity, particularly in the K^+ selective KcsA channel. One of these hypotheses is the so-called "field-strength hypothesis" which suggests that selectivity is determined by the type and the relative contribution of the coordinating ligand (e.g., protein versus water).[41,42] The idea behind this hypothesis is that different kinds of coordinating ligands will have differences in their intrinsic physical and electrostatic properties. Hence, the change in their relative contribution may result in a selectivity toward a particular ion. The "over-coordination hypothesis" attributes selectivity to the total number of coordinating ligands only and not their physical properties.[43,44] To perform a coordination number analysis, we followed the same procedure as reported previously for our WT simulations[19] (also see Supporting Information).

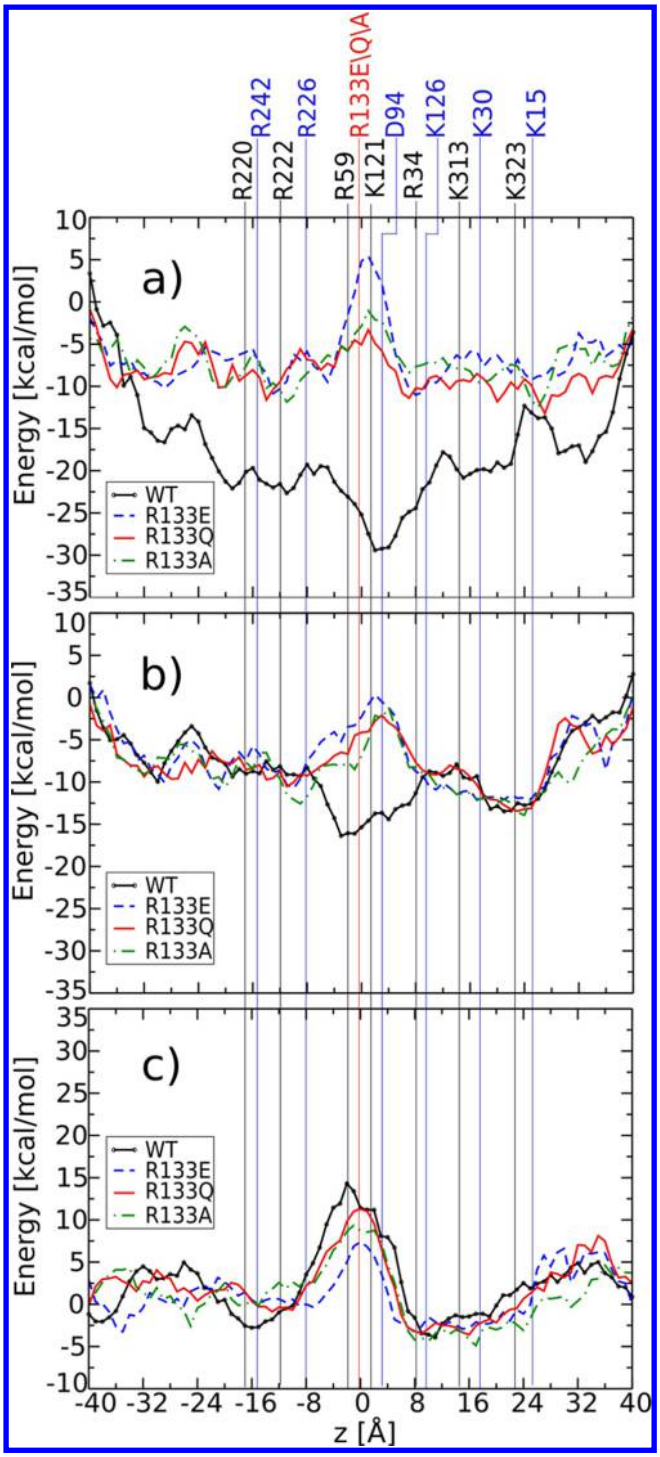

Figure 4. Electrostatic interaction energy for the (a) $H_2PO_4^-$, (b) Cl^-, and (c) K^+ ions passing through the OprP mutants R133E, R133Q, and R133A. For comparison, the electrostatic energy for the WT channel is also shown.[19] Important residues of OprP along the ion permeation pathway are mapped with respect to their position along the z axis. All energy values denote relative interaction energies assuming zero interaction energies in the bulk phase.

As a general trend and consistent with our previous results for WT OprP, the average number of coordinating water molecules decreased from the bulk phase as the ion moved inside the pore, which were compensated for by a higher number of protein contacts (Figure 5). The total number of coordinating ligands (water and protein contacts) remained

dx.doi.org/10.1021/bi400522b | Biochemistry 2013, 52, 5522−5532

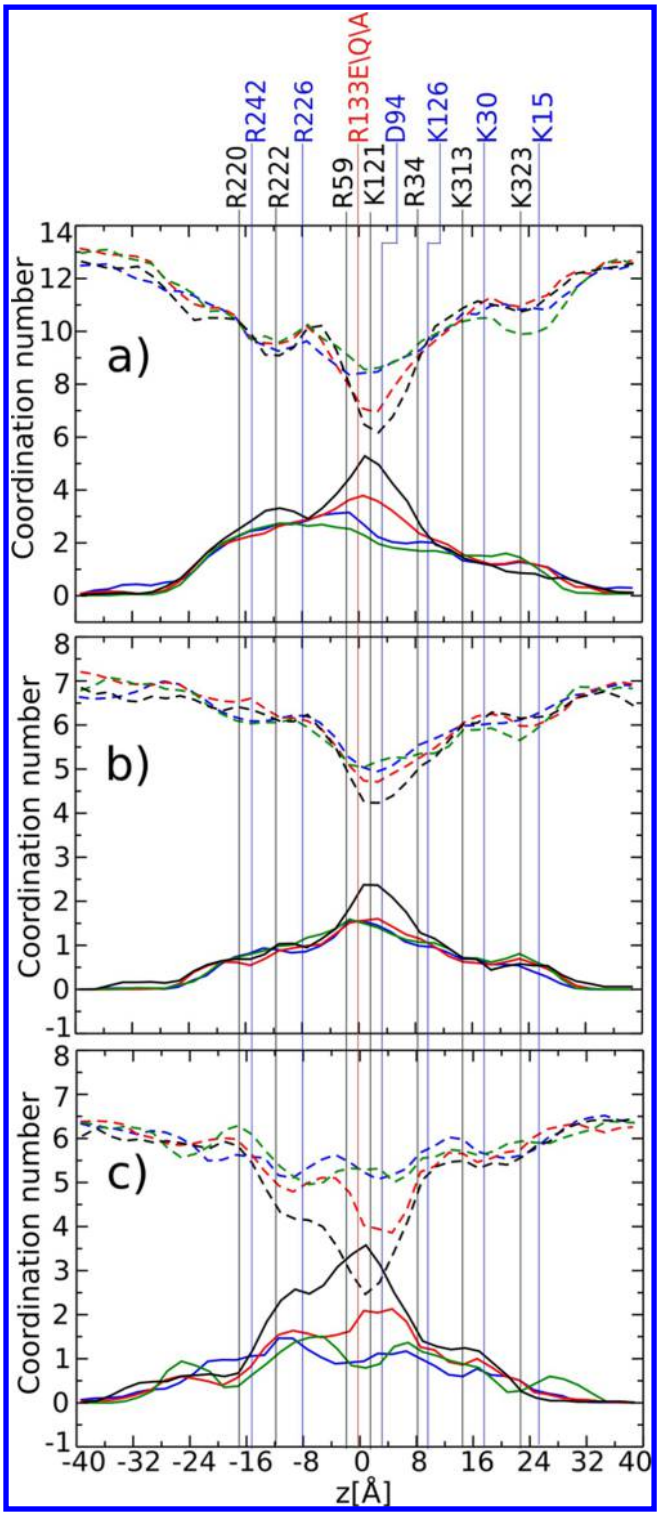

Figure 5. The coordination number, i.e., the water (dash line) and protein (solid line) contacts, for the different ions, (a) $H_2PO_4^-$, (b) Cl^-, and (c) K^+, through the OprP mutants channels R133E (blue), R133Q (red), and R133A (green). For comparison, the coordination numbers for the WT channel (black) are also shown.[19] Important residues of OprP along the ion permeation pathway are mapped with respect to their position along the *z* axis.

almost constant throughout the pore. Considering the above-discussed ion-selectivity hypotheses, the "over-coordination hypothesis" could not explain the selectivity of each of the ions for the WT OprP and different R133 mutants. Each ion had the same number of coordinating ligands among the WT OprP and different mutants; for example, $H_2PO_4^-$ had a coordination number of 13 for WT and R133E/Q/A. In contrast, the relative contributions (water versus protein contacts) varied for each ion among the WT and different mutants (Figure 5). For example, a phosphate ion (Figure 5a) has a different ratio of water versus protein contacts in the cases of WT OprP and the R133 mutants. The highest number of protein contacts is present in WT OprP. Hence, more water contacts are replaced by energetically favorable protein contacts in wildtype protein. This could explain the selectivity and higher binding affinity of phosphate for WT OprP compared to the R133 mutants, and this line of argument is in agreement with the "field-strength hypothesis".

In the central bindings sites, the $H_2PO_4^-$ ion transport through the WT pore indicated the removal of seven water molecules compared to the bulk phase which was compensated for by a higher number of protein contacts. As shown in Figure 5a, and different from the situation with WT OprP, the $H_2PO_4^-$ ions stripped six and four water molecules to enable passage through the R133Q and R133E/R133A pores, respectively. As a general trend, less water molecules were removed for all R133 mutants compared to the WT pore. R133 remained in contact with the $H_2PO_4^-$ ions in the entire central region in WT OprP simulations. A possible explanation for the removal of only four water molecules in the case of R133E might be the electrostatic repulsion between the negatively charged glutamate and the phosphate ion which in turn would lead to a loss of contacts between them. A closer contact between the R133 residue in WT channel and the negative ion would otherwise force water molecules to leave the phosphate hydration shell. A similar effect in R133A could be attributed to steric factors due to the small size of the alanine side chain. Figure 5b shows that the Cl^- transport through the R133 mutants revealed similar but somewhat more muted trends where less, i.e., two instead of three water molecules, were stripped compared to the WT channel.

The K^+ transport through the R133E mutant unfolded somewhat surprising results in terms of the coordination number. K^+ ions, being positively charged, were expected to strip more water molecules in the case of the R133E mutant compared to WT, due to the possible attractive electrostatic interactions between the ion and negatively charged glutamate (E). The same attractive interactions were responsible for stripping off more water molecules from $H_2PO_4^-$ in the WT pores due to favorable electrostatic interactions between the positively charge arginine and the negatively charged phosphate. Contrary to intuition, in the case of the cations also, the WT OprP removed more water molecules from the hydration shell than the R133E mutant. Indeed, R133E mutants stripped at maximum one water molecule compared to four in the WT case as seen in Figure 5c. As a general result, we observed that irrespective of the ion type (cation or anion), WT OprP could remove more water molecules from the hydration shell of the permeating ion than any of the studied R133 mutants.

Possible reasons for the unexpected behavior of the K^+ permeation through the R133E mutants in terms of coordination numbers were analyzed in further detail. The average distances were measured between the permeating K^+ ion and various residues of the WT as well as the R133E pore in the central region of the pore, i.e., between −6 Å to 6 Å. In the case of the WT channel, R133 and K^+ ions maintained very

dx.doi.org/10.1021/bi400522b | *Biochemistry* 2013, 52, 5522−5532

large distances between them, and they could not come closer than 7 Å (Figure 6). For the R133E mutant, E133 and K^+ came

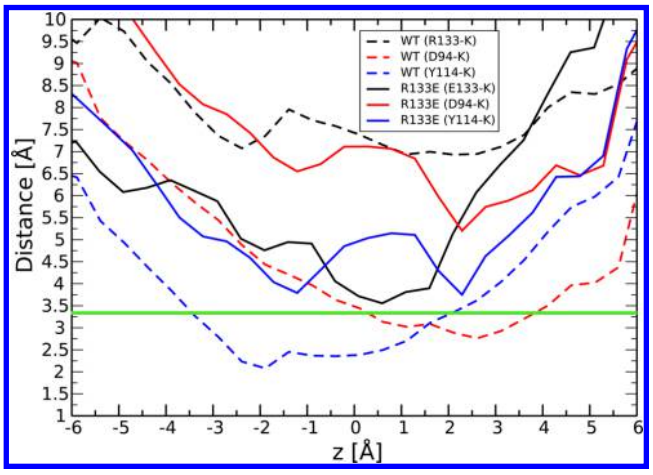

Figure 6. Average distances between a K^+ ion and terminal side chain atoms of residues R133/E133, D94, and Y114 from WT as well as the R133E mutant in the central regions of the OprP pore. The horizontal green line indicates the first hydration shell radius for K^+ ions. Average distances are measured with a bin width of 0.5 Å.

as close as 3.7 Å to each other, but this is not close enough to facilitate the removal of the majority number of water molecules from the first hydration shell since K^+ has a first hydration shell radius of 3.3 Å as indicated in Figure 6.

A detailed analysis of the binding site residues revealed that two residues, D94 (aspartate) and Y114 (tyrosine), were present at the wall opposite to R133/E133 (see Figure 1). For the WT channel, the strong electrostatic repulsion between R133 and the K^+ ion — having the closest distance of 7 Å — pushed the ion onto the wall at the opposite side and into close contact with D94 and Y114. The average distances between the permeating K^+ ions and these two residues are shown in Figure 6. The distances between the ions and D94/Y114 were small enough, i.e., as low as 2 Å, to facilitate removal of a first hydration shell water molecule from the K^+ ions. Different from WT results, in the case of the R133E mutant, D94/Y114 and the K^+ ions are at distances larger than the first hydration shell radius of the ion (see Figure 6). This might be due to the absence of any electrostatic repulsion between E133 residue in the mutant and K^+, contrary to the case for WT OprP. Furthermore, E133 and the K^+ ions did not experience strong enough attractive electrostatic interactions — having a closest distance of 3.7 Å — to facilitate removal of the large number of first hydration shell water of the ion. One of the possible reasons for the lack of such a strong attractive interaction between the K^+ ions and E133 could be the formation of a salt bridge between K121 (lysine) and E133, as observed in our simulations. Such a salt bridge is not possible between K121 and R133 in the case of the WT channel as they electrostatically repel each other.

The above analysis revealed one of the most important characteristics of the R133 residue of OprP in its ability to alter the solvation properties of permeating ions, and thereby indirectly regulate the selectivity and the ion transport properties of the pore. In the WT OprP, R133 has a clear preference to dehydrate the permeating ions, i.e., "drying out" effect, compared to the other residues in the mutants at this particular position. Taking advantage of its strategic position in OprP, its positive charge and large size, R133 has a tendency to "dry out" the permeating ions, both cations as well as anions. Thereby the R133 residue makes the ion more vulnerable to the channel environment in terms of various interactions. In the case of anions, it enforces "drying out" effects by an attractive electrostatic interactions, while in the case of cations it modifies their interactions with other residues (here D94 and Y114) via a strong electrostatic repulsion between the permeating cation and R133. Ion dehydration is an important property for the transport of ions through narrow channels.[45] Particularly for anion selective channels, e.g., Cl^- channels, the hydration energy of the permeating ions was reported to be the rate-limiting process in the ion transport.[46−48] In such a scenario, the importance of the R133 residue, due to its ability to dehydrate the ions, becomes even more evident in the anion-selective channel OprP. Consistent with this, previous single channel studies for OprP with anions of different sizes demonstrated a small increase in single channel conductance going from F^- to Cl^- and the subsequent linear decrease in the series Cl^-, Br^-, and I^- indicating that the hydration shell and size of the anions are important factors for the ion permeation through the channel.[49]

CONCLUSIONS

In our quest to achieve a detailed understanding of the structure−function relationship of OprP, and in continuation with our previous work on the WT pore, we have probed the ion selectivity of the OprP channel with a focus on an important central residue, R133. In this study, both electrophysiological measurements and free-energy MD simulations were carried out to investigate the role of R133 in determining phosphate binding specificity, ion selectivity and ion transport properties. To achieve this goal, three mutants were generated, namely, R133E, R133Q, and R133A, to understand the effect of charge and steric factors at this particular position of OprP. Electrophysiological measurements showed that any change in the R133 residue leads to a drastic reduction in the stability constant for phosphate binding. In qualitative agreement with experiments, PMF profiles obtained via MD simulations also indicated a change in the PMF profiles concerning the transport of phosphate from energetically favorable binding site regions for WT OprP to energetically unfavorable barrier regions for R133E/Q/A mutants. Furthermore, bilayer experiments revealed an extreme reduction in the pore KCl conductance and a reduced anion selectivity for all three R133 mutants compared to WT. The corresponding PMF profiles for K^+ and Cl^- transport through R133 mutants explained these observations from the experiments. In addition, taking advantage of the atomic details provided by the MD simulations, we observed the important characteristic of the R133 residue in OprP to alter the solvation property of the permeating ion via its ability to dehydrate the ion and thereby controlling the molecular interactions of the ions with the pore. Our study reveals the role of the R133 residue — particularly its charge and ability to change the solvation behavior of the permeating ion — in the structure−function relationship of OprP. This kind of detailed information can be further exploited to understand the ion selectivity of other pores and nanochannels and to enable the design of ion-selective artificial nanopores as, for example, proposed in ref 21.

dx.doi.org/10.1021/bi400522b | *Biochemistry* 2013, 52, 5522−5532

■ ASSOCIATED CONTENT

Supporting Information

Multiple sequence alignment among OprP orthologs in different *Pseudomonas* species, RDF profiles for ion hydration number, and PMF profiles with error bars are presented. This material is available free of charge via the Internet at http://pubs.acs.org.

■ AUTHOR INFORMATION

Corresponding Author

*E-mail: u.kleinekathoefer@jacobs-university.de. Phone: +49 (0)421 200 3523.

Funding

The research leading to these results has received support from the Innovative Medicines Joint Undertaking under Grant Agreement No. 115525, resources which are composed of financial contributions from the European Union's seventh framework program (FP7/2007−2013) and EFPIA companies in kind contribution. This work has also been supported by Grants KL 1299/6-1 and BE 865/16-1 of the Deutsche Forschungsgemeinschaft (DFG) and a Canadian Institutes for Health Research grant to R.E.W.H. who also has a Canada Research Chair in Health and Genomics.

Notes

The authors declare no competing financial interest.

■ ACKNOWLEDGMENTS

The authors would like to thank Que-Tien Tran for her contribution at the early stage of this study.

■ REFERENCES

(1) Benz, R., Ed. (2004) *Bacterial and Eukaryotic Porins*, Wiley-VCH, Weinheim.

(2) Howorka, S., and Siwy, Z. (2009) Nanopore analytics: sensing of single molecules. *Chem. Soc. Rev. 38*, 2360−2384.

(3) Siwy, Z. S., and Howorka, S. (2010) Engineered voltage-responsive nanopores. *Chem. Soc. Rev. 39*, 1115−1132.

(4) Aksimentiev, A., and Schulten, K. (2005) Imaging alpha-hemolysin with molecular dynamics: ionic conductance, osmotic permeability, and the electrostatic potential map. *Biophys. J. 88*, 3745−3751.

(5) Pezeshki, S., Chimerel, C., Bessenov, A., Winterhalter, M., and Kleinekathöfer, U. (2009) Understanding ion conductance on a molecular level: An all-atom modeling of the bacterial porin OmpF. *Biophys. J. 97*, 1898−1906.

(6) Biro, I., Pezeshki, S., Weingart, H., Winterhalter, M., and Kleinekathöfer, U. (2010) Comparing the Temperature-Dependent Conductance of the Two Structurally Similar *E. coli* Porins OmpC and OmpF. *Biophys. J. 98*, 1830−1839.

(7) Modi, N., Singh, P. R., Mahendran, K. R., Schulz, R., Winterhalter, M., and Kleinekathöfer, U. (2011) Probing the Transport of Ionic Liquids in Aqueous Solution Through Nanopores. *J. Phys. Chem. Lett. 2*, 2331−2336.

(8) Modi, N., Winterhalter, M., and Kleinekathöfer, U. (2012) Computational modeling of ion transport through nanopores. *Nanoscale 4*, 6166−6180.

(9) Maffeo, C., Bhattacharya, S., Yoo, J., Wells, D., and Aksimentiev, A. (2012) Modeling and Simulation of Ion Channels. *Chem. Rev. 112*, 6250−6284.

(10) Mach, T., Neves, P., Spiga, E., Weingart, H., Winterhalter, M., Ruggerone, P., Ceccarelli, M., and Gameiro, P. (2008) Facilitated permeation of antibiotics across membrane channels-interaction of the quinolone moxifloxacin with the OmpF channel. *J. Am. Chem. Soc. 130*, 13301−13309.

(11) Mahendran, K. R., Hajjar, E., Mach, T., Lovelle, M., Kumar, A., Sousa, I., Spiga, E., Weingart, H., Gameiro, P., Winterhalter, M., and Ceccarelli, M. (2010) Molecular basis of enrofloxacin translocation through OmpF, an outer membrane channel of *Escherichia coli*—when binding does not imply translocation. *J. Phys. Chem. B 114*, 5170−5179.

(12) Hajjar, E., Mahendran, K. R., Kumar, A., Bessonov, A., Petrescu, M., Weingart, H., Ruggerone, P., Winterhalter, M., and Ceccarelli, M. (2010) Bridging timescales and length scales: from macroscopic flux to the molecular mechanism of antibiotic diffusion through porins. *Biophys. J. 98*, 569−575.

(13) Raj Singh, P., Ceccarelli, M., Lovelle, M., Winterhalter, M., and Mahendran, K. R. (2012) Antibiotic Permeation across the OmpF Channel: Modulation of the Affinity Site in the Presence of Magnesium. *J. Phys. Chem. B 116*, 4433−4438.

(14) Hancock, R. E. W., Poole, K., and Benz, R. (1982) Outer membrane protein P of Pseudomonas aeruginosa: regulation by phosphate deficiency and formation of small anion-specific channels in lipid bilayer membranes. *J. Bacteriol. 150*, 730−738.

(15) Moraes, T., Bains, M., Hancock, R. E. W., and Strynadka, N. (2006) An arginine ladder in OprP mediates phosphate-specific transfer across the outer membrane. *Nat. Struct. Mol. Biol. 14*, 85−87.

(16) Benz, R., Egli, C., and Hancock, R. E. W. (1993) Anion transport through the phosphate-specific OprP-channel of the Pseudomonas aeruginosa outer membrane: effects of phosphate, di- and tribasic anions and of negatively-charged lipids. *Biochim. Biophys. Acta 1149*, 224−230.

(17) Benz, R., and Hancock, R. E. W. (1987) Mechanism of ion transport through the anion-selective channel of the Pseudomonas aeruginosa outer membrane. *J. Gen. Physiol. 89*, 275−295.

(18) Hancock, R. E. W., and Benz, R. (1986) Demonstration and chemical modification of a specific phosphate binding site in the phosphate-starvation-inducible outer membrane porin protein P of Pseudomonas aeruginosa. *Biochim. Biophys. Acta 860*, 699−707.

(19) Modi, N., Benz, R., Hancock, R. E. W., and Kleinekathöfer, U. (2012) Modeling the Ion Selectivity of the Phosphate Specific Channel OprP. *J. Phys. Chem. Lett. 3*, 3639−3645.

(20) Pongprayoon, P., Beckstein, O., Wee, C. L., and Sansom, M. S. (2009) Simulations of anion transport through OprP reveal the molecular basis for high affinity and selectivity for phosphate. *Proc. Natl. Acad. Sci. U. S. A. 106*, 21614−21618.

(21) Pongprayoon, P., Beckstein, O., and Sansom, M. S. P. (2011) Biomimetic Design of a Brush-Like Nanopore: Simulation Studies. *J. Phys. Chem. B 116*, 462−468.

(22) Sukhan, A., and Hancock, R. E. W. (1995) Insertion mutagenesis of the Pseudomonas aeruginosa phosphate-specific porin OprP. *J. Bacteriol. 177*, 4914−4920.

(23) Bauer, K., Struyve, M., Bosch, D., Benz, R., and Tommassen, J. (1989) One single lysine residue is responsible for the special interaction between polyphosphate and the outer membrane porin PhoE of *Escherichia coli*. *J. Biol. Chem. 264*, 16393−16398.

(24) Benz, R., Janko, K., and Lauger, P. (1979) Ionic selectivity of pores formed by the matrix protein (porin) of *Escherichia coli*. *Biochim. Biophys. Acta 551*, 238−247.

(25) Benz, R., Schmid, A., and Vos-Scheperkeuter, G. H. (1987) Mechanism of sugar transport through the sugar-specific LamB channel of *Escherichia coli* outer membrane. *J. Membr. Biol. 100*, 21−29.

(26) Benz, R., Schmid, A., Nakae, T., and Vos-Scheperkeuter, G. (1986) Pore formation by LamB of *Escherichia coli* in lipid bilayer membranes. *J. Bacteriol. 165*, 978−986.

(27) Thein, M., Bonde, M., Bunikis, I., Denker, K., Sickmann, A., Bergström, S., and Benz, R. (2012) DipA, a pore-forming protein in the outer membrane of lyme disease spirochetes exhibits specificity for the permeation of dicarboxylates. *PLoS One 7*, e36523.

(28) Ludwig, O., De Pinto, V., Palmieri, F., and Benz, R. (1986) Pore formation by the mitochondrial porin of rat brain in lipid bilayer membranes. *Biochim. Biophys. Acta 860*, 268.

(29) Humphrey, W. F., Dalke, A., and Schulten, K. (1996) VMD − Visual Molecular Dynamics. *J. Mol. Graph. 14*, 33−38.
(30) Phillips, J. C., Braun, R., Wang, W., Gumbart, J., Tajkhorshid, E., Villa, E., Chipot, C., Skeel, R. D., Kale, L., and Schulten, K. (2005) Scalable molecular dynamics with NAMD. *J. Comput. Chem. 26*, 1781−1802.
(31) MacKerell, A. (1998) All-Atom Empirical Potential for Molecular Modeling and Dynamics Studies of Proteins. *J. Phys. Chem. B 102*, 3586−3616.
(32) Kleinekathöfer, U., Isralewitz, B., Dittrich, M., and Schulten, K. (2011) Domain motion of individual F_1-ATPase β-subunits during unbiased molecular dynamics simulations. *J. Phys. Chem. A 115*, 7267−7274.
(33) Darden, T., York, D., and Pedersen, L. (1993) Particle mesh Ewald: An N log (N) method for Ewald sums in large systems. *J. Chem. Phys. 98*, 10089−10089.
(34) Tuckerman, M., Berne, B., and Martyna, G. (1992) Reversible multiple time scale molecular dynamics. *J. Chem. Phys. 97*, 1990−2001.
(35) Ryckaert, J.-P., Ciccotti, G., and Berendsen, H. J. C. (1977) Numerical integration of the cartesian equations of motion of a system with constraints: molecular dynamics of n-alkanes. *J. Comput. Phys. 23*, 327−341.
(36) Darve, E., and Pohorille, A. (2001) Calculating free energies using average force. *J. Chem. Phys. 115*, 9169−9183.
(37) Hénin, J., and Chipot, C. (2004) Overcoming free energy barriers using unconstrained molecular dynamics simulations. *J. Chem. Phys. 121*, 2904−2914.
(38) Hénin, J., Fiorin, G., Chipot, C., and Klein, M. L. (2010) Exploring Multidimensional Free Energy Landscapes Using Time-Dependent Biases on Collective Variables. *J. Chem. Theory Comput. 6*, 35−47.
(39) Allen, T. W., Andersen, O. S., and Roux, B. (2006) Ion permeation through a narrow channel: using gramicidin to ascertain all-atom molecular dynamics potential of mean force methodology and biomolecular force fields. *Biophys. J. 90*, 3447−3448.
(40) Chang, C., Chen, W., and Gilson, M. (2007) Ligand configurational entropy and protein binding. *Proc. Natl. Acad. Sci. U. S. A. 104*, 1534−1539.
(41) Egwolf, B., and Roux, B. (2010) Ion selectivity of the KcsA channel: a perspective from multi-ion free energy landscapes. *J. Mol. Biol. 401*, 831−842.
(42) Noskov, S., Bernéche, S., and Roux, B. (2004) Control of ion selectivity in potassium channels by electrostatic and dynamic properties of carbonyl ligands. *Nature 431*, 830−834.
(43) Varma, S., and Rempe, S. (2007) Tuning ion coordination architectures to enable selective partitioning. *Biophys. J. 93*, 1093−1099.
(44) Thomas, M., Jayatilaka, D., and Corry, B. (2007) The predominant role of coordination number in potassium channel selectivity. *Biophys. J. 93*, 2635−2643.
(45) Richards, L. A., Schäfer, A. I., Richards, B. S., and Corry, B. (2012) The importance of dehydration in determining ion transport in narrow pores. *Small 8*, 1701−1709.
(46) Bormann, J., Hamill, O., and Sakmann, B. (1987) Mechanism of anion permeation through channels gated by glycine and gamma-aminobutyric acid in mouse cultured spinal neurones. *J. Physiol. (Lond.) 385*, 243−286.
(47) Verdon, B., Winpenny, J., Whitfield, K., Argent, B., and Gray, M. (1995) Volume-activated chloride currents in pancreatic duct cells. *J. Membr. Biol. 147*, 173−183.
(48) Linsdell, P., and Hanrahan, J. (1998) Adenosine triphosphate-dependent asymmetry of anion permeation in the cystic fibrosis transmembrane conductance regulator chloride channel. *J. Gen. Physiol. 111*, 601−614.
(49) Benz, R., Poole, K., and Hancock, R. E. W. (1984) Characterization and Chemical Modification of Small Anion Specific Channels formed in Lipid Bilayer Membranes by Outer Membrane Protein P of Pseudomonas aeruginosa. *Biophys. J. 45*, 81−82.